Effect of the support domain size in SPH fracture simulations

Martin Hušek, Jiří Kala, Petr Král, and Filip Hokeš

***Abstract*—** The simulation of numerical methods is accompanied by problems caused by false dependencies arising from the mathematical basis of such methods. The use of the Smoothed Particle Hydrodynamics (SPH) method removes the problems caused by the presence of a physical mesh that occur, e.g. when the Finite Element Method (FEM) is used. Although meshfree methods are generally less likely to produce false numerical dependencies, in some cases certain measures must be taken in order to avoid obtaining unexpected results. In the case of the SPH this necessarily involved the regular distribution of particles in discretized domains. This contribution describes a fracture mechanics experiment in which L-shaped concrete specimens undergo dynamic fracture. The experiment is simulated via the SPH method, during which clusters of particles are artificially created so that the resulting distribution in the discretized domain (or a zone within it) is irregular. The consequences of this irregularity and its effect on the form of failure are studied along with possible ways in which false (dependent) behaviour can be prevented. The results from the SPH method are also compared to FEM results.

***Keywords*—**Concrete, dynamic fracture, nonlinear constitutive model, smoothed particle hydrodynamics, support domain.

I. Introduction

MANY structures of high importance to society are designed using the principle of a skeleton, which is the main load-bearing part of the structure. The skeleton can be created as a series of spatially connected frames. Most frequently, structural steel or reinforced concrete is used as the building material for the primary load-bearing system. Each of these construction materials has its advantages and disadvantages – mainly during dynamic loading. Thanks to the high strength of steel, structures can be designed very economically. This can result in structures within which thin profiles are predominant. Despite their possible high load-bearing capacity, such profiles are very prone to stability loss [1]–[3]. Indeed, whole frames can lose stability due to imperfections arising during production [4].

In the case of concrete structures, loss of stability is not necessarily a problem. This is frequently thanks to their robustness, which stems from the lower load-bearing capacity of concrete in contrast with structural steel – the profiles used in structures must be more massive. However, negative aspects of the robustness of concrete start to appear when dynamic loading (e.g. seismicity) takes place. The occurrence of cracks is very frequent in the area of rigid frame joints. Of course, problems involving damage as a result of seismic activity also affect steel structures [5]. Loading does not necessarily have to be only of a natural character – quite the opposite. The question arises more and more frequently as to whether a structure should also be built to withstand intentional loading (e.g. plane crashes or explosions); see also [6]–[8]. It is obvious that deciding which specific material to choose is not a simple matter. Concrete (and its reinforced variants) is often chosen for its wide variability.

With regard to the frequent complexity of structures, concrete as a construction material and the type of loading itself, it is not possible to design a structure without the execution of a simulation or numerical analysis. One of the most widely used numerical methods for the solution of complex issues is the Finite Element Method (FEM). In cases when the calculation also includes the aforementioned rigid frame joints, the FEM does not lead to correct results, particularly in cases of high-speed stress. Despite the availability of various material models of concrete [9], [10], which can be used to improve initial parameter optimization processes when needed [11], the acquisition of correct results can be very difficult when using the FEM method [12], or impossible in certain cases [13].

The answer to the question of how to successfully simulate a concrete frame joint exposed to high-speed stress can be found using the Smoothed Particle Hydrodynamics (SPH) method. This meshfree method differs from the FEM in that it operates without a physical mesh (or the physical connection of individual particles). It can deal with problems involving large

This outcome has been achieved with the financial support of project GACR 14-25320S "Aspects of the use of complex nonlinear material models" provided by the Czech Science Foundation; with the support of the project FAST-S-16-3718 "Advanced numerical methods with complex material models" provided by the Brno University of Technology fund for specific university research; and also with the support of the project LO1408 "AdMaS UP – Advanced Materials, Structures and Technologies" provided by the Ministry of Education, Youth and Sports under the „National Sustainability Programme I".

M. Hušek is with the Faculty of Civil Engineering, Institute of Structural Mechanics, Brno University of Technology, Czech Republic (e-mail: husek.m@fce.vutbr.cz).

J. Kala is with the Faculty of Civil Engineering, Institute of Structural Mechanics, Brno University of Technology, Czech Republic (e-mail: kala.j@fce.vutbr.cz).

P. Král is with the Faculty of Civil Engineering, Institute of Structural Mechanics, Brno University of Technology, Czech Republic (e-mail: kral.p@fce.vutbr.cz).

F. Hokeš is with the Faculty of Civil Engineering, Institute of Structural Mechanics, Brno University of Technology, Czech Republic (e-mail: hokes.f@fce.vutbr.cz).

deformations, including the resultant fragmentation of matter, without any major problems [14]. However, in cases when the distribution of SPH particles of the original geometry is not regular, the results do not correspond with those from experiments. The size of this problem is also influenced by the density of the discretization of the continuum.

In order to evaluate these dependencies, the contribution focuses on dynamic loading issues concerning concrete L-specimens which are simulated using the SPH method. In the executed simulations, the regularity of the distribution of SPH particles and its influence on the type of failure are primarily examined. Results from FEM simulations and experiments are used for comparison.

II. Essential Formulation of the SPH

The formulation of the SPH method is often divided into two key steps. The first step is the *integral representation* of field functions, and the second is *particle approximation*. The concept of the integral representation of a function $f(\boldsymbol{x})$ used in the SPH method starts from the following identity:

$$f(\boldsymbol{x}) = \int_{\Omega} f(\boldsymbol{x}')\delta(\boldsymbol{x}-\boldsymbol{x}')\,d\boldsymbol{x}' \tag{1}$$

where f is a function of the three-dimensional position vector $\boldsymbol{x}$, and $\delta(\boldsymbol{x}-\boldsymbol{x}')$ is the Dirac delta function given by

$$\delta(\boldsymbol{x}-\boldsymbol{x}') = \begin{cases} +\infty & \boldsymbol{x} = \boldsymbol{x}' \\ 0 & \boldsymbol{x} \neq \boldsymbol{x}' \end{cases} \tag{2}$$

In (1), Ω is the volume of the integral that contains $\boldsymbol{x}$. Equation (1) implies that a function can be represented in an integral form. Since the Dirac delta function is used, the integral representation in (1) is exact or rigorous as long as $f(\boldsymbol{x})$ is defined and continuous in Ω [15]. If the Delta function $\delta(\boldsymbol{x}-\boldsymbol{x}')$ is replaced by a smoothing function $W(\boldsymbol{x}-\boldsymbol{x}', h)$, the integral representation of $f(\boldsymbol{x})$ is given by

$$f(\boldsymbol{x}) \approx \int_{\Omega} f(\boldsymbol{x}')W(\boldsymbol{x}-\boldsymbol{x}', h)\,d\boldsymbol{x}' \tag{3}$$

where W is the so-called smoothing function and h is the smoothing length defining the influence area of the smoothing function W. Note that as long as W is not the Dirac delta function, the integral representation in (3) can only be an approximation [15]. The continuous integral representations concerning the SPH integral approximation in (3) can be converted into discretized forms of summation over all the particles in the support domain shown in Fig. 1. The corresponding discretized process of summation over the particles is commonly known as particle approximation. If the infinitesimal volume $d\boldsymbol{x}'$ in (3) at the location of particle j is replaced by the finite volume of the particle ΔV_j that is related to the mass of the particles m_j by

$$m_j = \Delta V_j \rho_j \tag{4}$$

where ρ_j is the density of particle j (= 1, 2,…, N) in which N is the number of particles within the support domain of particle j, then the continuous SPH integral representation for $f(\boldsymbol{x})$ can be written in the following form of discretized particle approximation [15]:

$$\begin{aligned} f(\boldsymbol{x}) &\approx \int_{\Omega} f(\boldsymbol{x}')W(\boldsymbol{x}-\boldsymbol{x}', h)\,d\boldsymbol{x}' \\ &\approx \sum_{j=1}^{N} f(\boldsymbol{x}_j)W(\boldsymbol{x}-\boldsymbol{x}_j, h)\Delta V_j \\ &\approx \sum_{j=1}^{N} f(\boldsymbol{x}_j)W(\boldsymbol{x}-\boldsymbol{x}_j, h)\frac{1}{\rho_j}(\rho_j \Delta V_j) \\ &\approx \sum_{j=1}^{N} f(\boldsymbol{x}_j)W(\boldsymbol{x}-\boldsymbol{x}_j, h)\frac{1}{\rho_j}(m_j) \end{aligned} \tag{5}$$

or just

$$f(\boldsymbol{x}_i) \approx \sum_{j=1}^{N} \frac{m_j}{\rho_j} f(\boldsymbol{x}_j)W(\boldsymbol{x}_i-\boldsymbol{x}_j, h) \tag{6}$$

Equation (6) states that the value of a function at particle i is approximated using the average of those values of the function at all the particles in the support domain of particle i weighted by the smoothing function shown in Fig. 1.

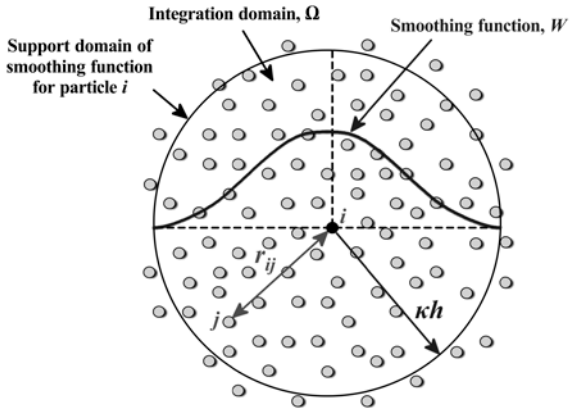

Fig. 1. Particle approximations using particles within the support domain of the smoothing function W for particle i.

A. Problem with the support domain

The extent of the support domain is defined according to Fig. 1 as the size of the generally variable parameter h, which is called the smoothing length. Parameter h can also be multiplied by constant κ. Particles which are inside the support domain attributable to particle i are called neighbouring particles. If the resultant value of the product κh in each time step of the numerical simulation is the same, there can be the decrease in the number of neighbouring particles and thus also the decrease in the accuracy of the solution due the effect of excessive deformations (i.e. during the mutual divergence of the SPH particles). It is advisable to change the size of the

support domain during the calculation in such a way that the number of neighbouring particles is constant.

There are many ways to dynamically develop *h* so that the number of neighbouring particles remains relatively constant. In 1989, Benz [16] suggested a method of developing the smoothing length. This method uses the time derivative of the smoothing function in terms of the continuity equation

$$\frac{dh}{dt} = -\frac{1}{d}\frac{h}{\rho}\frac{d\rho}{dt} = \frac{1}{d}h\nabla\cdot\boldsymbol{v} \tag{7}$$

where d is the number of dimensions and $\nabla\cdot\boldsymbol{v}$ is the divergence of the flow. This means that the smoothing length increases when particles separate from each other and reduces when the concentration of particles is significant; see Fig. 2. It varies in order to keep the same number of particles in the neighbourhood. Equation (7) can be discretized using SPH approximations and calculated with other differential equations in parallel [15].

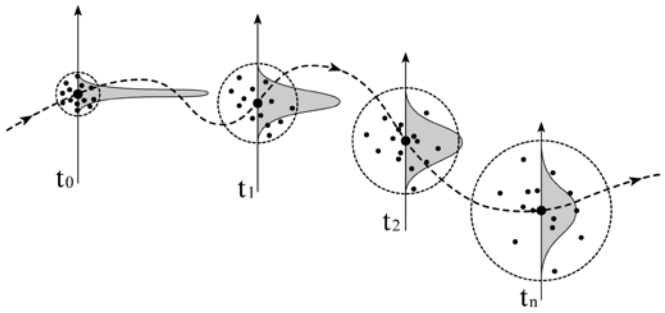

Fig. 2. Evolution of the support domain during the simulation. Smoothing length increases when particles separate from each other.

III. Experiment

In 2015, Ožbolt *et al.* [17] carried out experiments during which he controlled the displacement of L-shaped concrete specimens at different speeds. The aim of the experiments and subsequent numerical simulations was to discover the dependencies between the material strength and the loading speed.

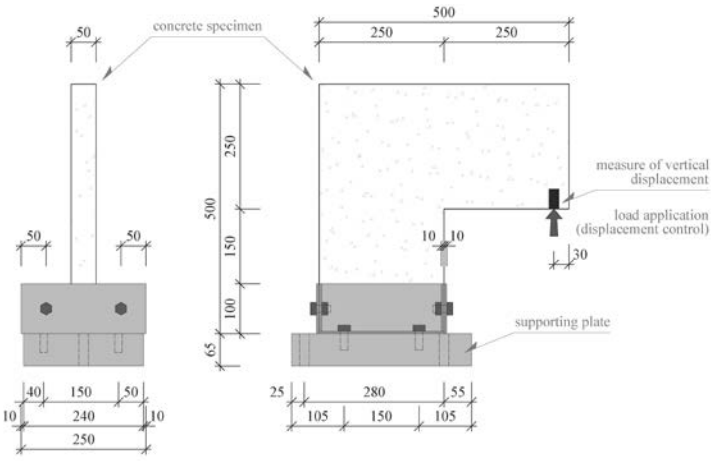

Fig. 3. Geometry and boundary conditions of the L-specimen (units in mm) [17].

Even though displacement control speeds of 0.25 mms^{-1}-2400 mms^{-1} were tested in the experiment, this contribution only requires attention to be paid to the highest loading speed, i.e. 2400 mms^{-1}. Fig. 3 shows a diagram of the placement of concrete specimens from the executed experiment.

Fig. 4 depicts type of failure at loading speed of 2400 mms^{-1}. In the experiment the type of failure changed due to the effect of loading speed [17]. With the change in loading speed, the resistance of the concrete specimen against deformation also changed, as did the measured maximum resistance strength – peak load. 127.73 kN was measured for a loading speed of 2400 mms^{-1}.

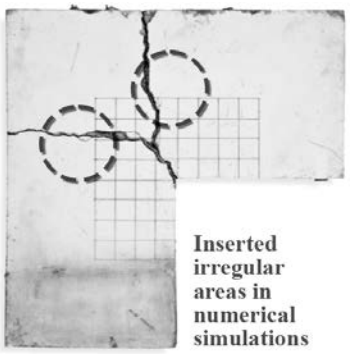

Fig. 4. Failure type for displacement loading speed of 2400 ms^{-1} [17].

IV. SPH and FEM Simulations

The aim of carrying out numerical simulations using the SPH method was to achieve the values measured in the experiment (for a loading speed of 2400 mms^{-1}). It was also used to obtain a corresponding failure mode to that which can be seen in Fig. 4. Simulations were carried out also using the FEM method in order to check the SPH method's results. The initial geometry and placement were always the same (for all discretization variants), as can be seen in Fig. 3. Simulations were performed in the LS-DYNA program [18].

A. Material model of concrete

In the numerical simulations, only the concrete specimen without steel brackets was modelled. This was done to minimize possible numerical instabilities (e.g. contacts between steel and concrete). In this way, attention could be focused exclusively on the behaviour of the SPH method. The Continuous Surface Cap Model (CSCM) was chosen as the material model of concrete to be used [19], [20]. Table I shows the parameters used in the simulations.

TABLE I
THE MATERIAL PARAMETERS FOR THE CSCM MODEL

Mass density, ρ_c (kgm^{-3})	2210
Compressive strength, f_c (MPa)	46.25
Tensile strength, f_t (MPa)	3.12
Young's modulus, E_c (GPa)	32.2
Poisson's ratio, v_c	0.18
Fracture energy, G_F (Jm^{-2})	58.56
Maximum aggregate size, a_g (mm)	8

B. From FEM to SPH

So that the results of the simulations of the FEM and SPH methods could be compared, FEM mesh was used as the basis for the creation of the SPH model. SPH particles were placed in the center of gravity of the FEM elements.

V. Simulation Results

In the first results section, the functionality of the FEM and SPH methods is tested for a regular mesh with different division densities. In the second results section, an area (cluster) with a rougher division is inserted into the original mesh (with the finest division). In addition, this area is intentionally placed at locations through which the crack is supposed to pass; see Fig. 4.

A. Regular mesh and density of spatial discretization

Discretization sizes of 16.66 mm, 10 mm and 6.25 mm were chosen for the FEM elements. In this way, division into 3, 5 and 8 elements were achieved along the thickness of the concrete specimen. As the SPH particles were created from FEM elements, the distances between them were also 16.66 mm, 10 mm and 6.25 mm. Fig. 5 and Table II show the results for a regular FEM mesh and the distribution of SPH particles. The results correspond well with the experiments.

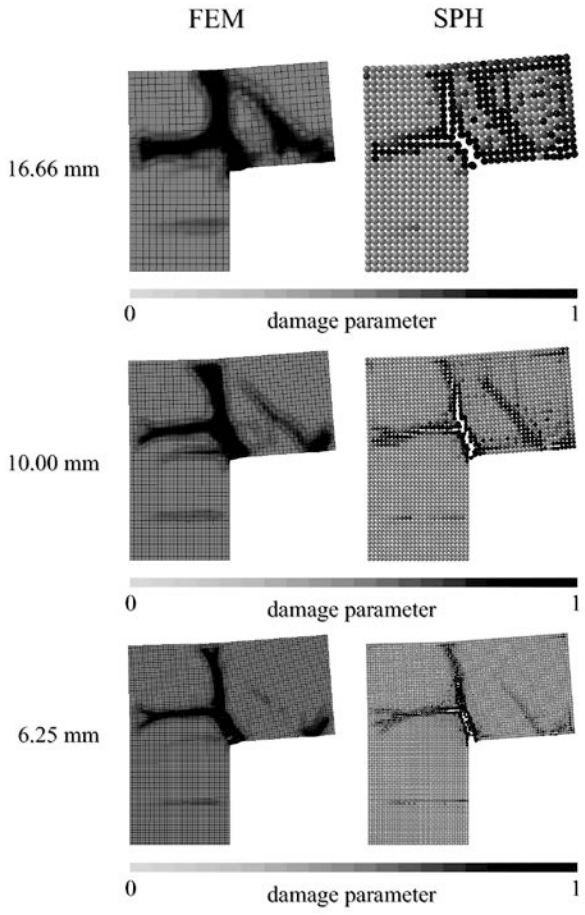

Fig. 5. Regular FEM mesh and SPH particle distribution results.

Table II
The peak load for regular FEM mesh and SPH particle distribution

Size	FEM	SPH	experiment
16.66 mm	123.07 kN	121.06 kN	
10.00 mm	126.78 kN	123.07 kN	127.73 kN
6.25 mm	130.08 kN	124.18 kN	

B. Irregular mesh and κ parameter influence

In the second case, zones (clusters) were inserted into the numerical model with element sizes of 6.25 mm where the size of the FEM mesh or the distance between the SPH particles was increased to 12.5 mm, i.e. 2x greater. With regard to this, an irregular zone of transition from size 6.25 mm to 12.5 mm was also created.

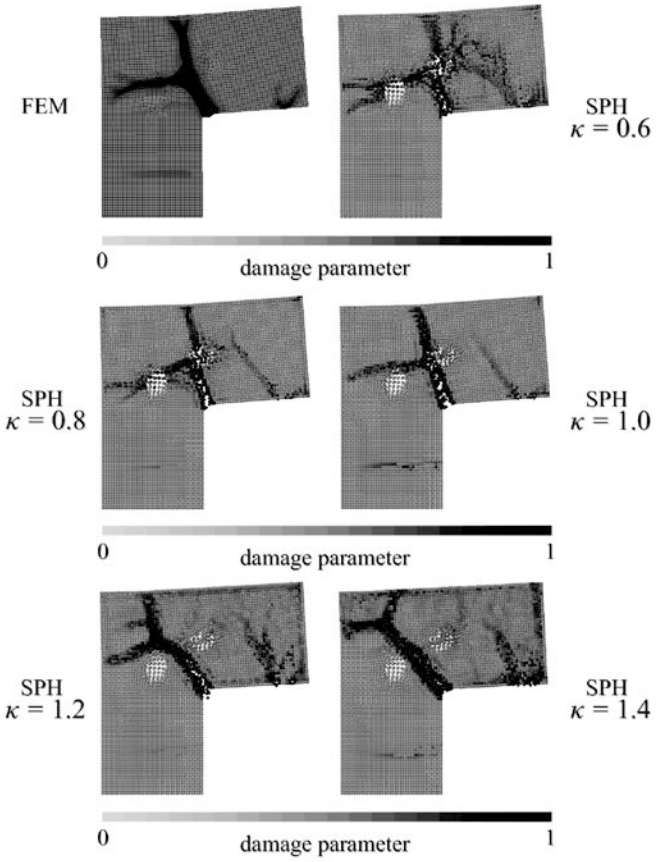

Fig. 6. Irregular FEM mesh and SPH particle distribution results. Distance between SPH particles in cluster 12.5 mm.

Table III
The peak load for irregular FEM mesh and SPH particle distribution distance between SPH particles in cluster 12.5 mm

Parameter κ	FEM	SPH	experiment
0.6		136.00 kN	
0.8		117.39 kN	
1.0	129.13 kN	100.03 kN	127.73 kN
1.2		76.38 kN	
1.4		44.68 kN	

Fig. 6 and Table III show the results for an irregular FEM mesh and the distribution of SPH particles. Even though the results of the FEM simulation show that the inserted irregular area (clusters) does not have a significant influence either on the size of the peak load or the shape of the failure, the result is strongly dependent on the selected parameter κ in the case of the SPH method, i.e. on the size of the support domain. In the case $\kappa = 1$ it is obvious that the cracks avoid inserted clusters with rougher division. Moreover, the measured strength does not correspond to the experiment. With increasing values of κ, the simulation results are increasingly different from the results of the experiment. The value $\kappa < 1$ then shows a better correspondence between the simulation and the experiment. The optimum value of κ according to Table III appears to be $\kappa \approx 0.7$.

VI. Finding the *K* Trend

Although the application of linear modification (7) produces good results and corresponds with the experiment, this may not always happen if irregularity is more significant (i.e. with continuously increasing differences in distances between particles within a cluster, and outside it). As a result, attempts were made to find the κ trend for additional configurations in which the intracluster distances between particles changed further.

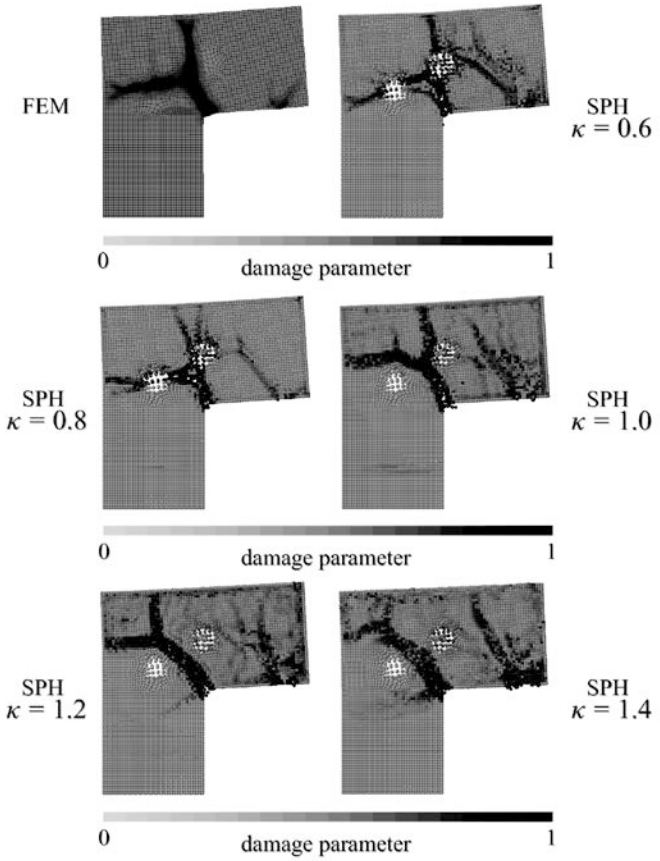

Fig. 7. Irregular FEM mesh and SPH particle distribution results. Distance between SPH particles in cluster 14.44 mm.

A. Highlighting of irregularity

The highlighting of irregularity (heterogeneity) was carried out by increasing the intracluster distances between SPH particles. The size of the zone of irregularity was maintained, however; see Fig. 4. Fig. 7 shows the results for intracluster particle distances of 14.44 mm. Subsequently, Fig. 8 contains results for distances of 16.66 mm. In both cases, the same (or markedly similar) phenomenon occurs as with the first tested case; see Fig. 6. Again, crack development for the values $\kappa = 1$ does not correspond with the experiment results.

Table IV
The peak load for irregular FEM mesh and SPH particle distribution distance between SPH particles in cluster 14.44 mm

Parameter κ	FEM	SPH	experiment
0.6		131.79 kN	
0.8		112.67 kN	
1.0	128.18 kN	89.02 kN	127.73 kN
1.2		57.05 kN	
1.4		32.43 kN	

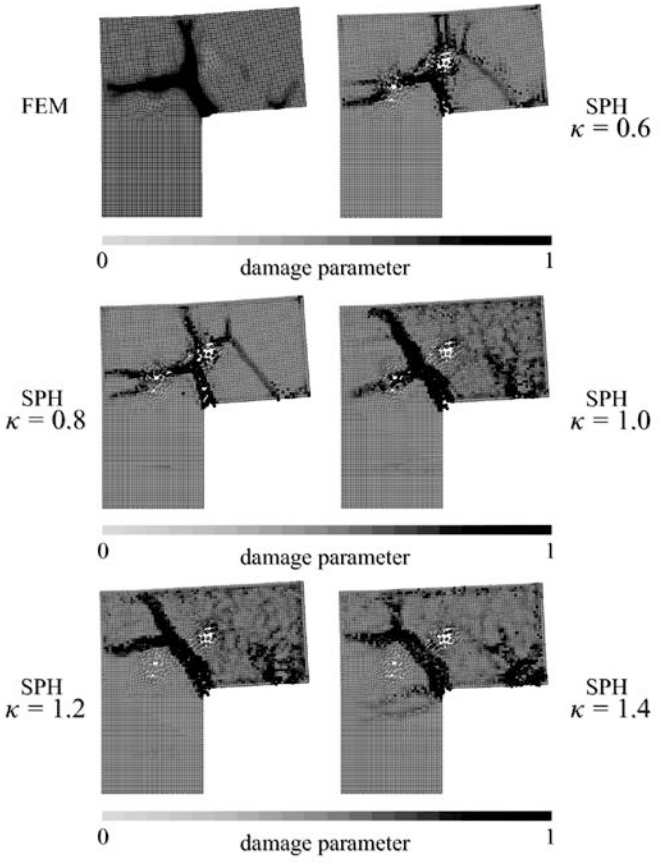

Fig. 8. Irregular FEM mesh and SPH particle distribution results. Distance between SPH particles in cluster 16.66 mm.

In addition, at values of $\kappa \geq 1$, higher failure values appear in the loaded area. The authors believe this phenomenon is due to the size of the transition that appears between the area of irregularity and the rest of the model.

TABLE V
THE PEAK LOAD FOR IRREGULAR FEM MESH AND SPH PARTICLE DISTRIBUTION
DISTANCE BETWEEN SPH PARTICLES IN CLUSTER 16.66 MM

Parameter κ	FEM	SPH	experiment
0.6		130.64 kN	
0.8		110.74 kN	
1.0	126.13 kN	87.58 kN	127.73 kN
1.2		54.58 kN	
1.4		31.88 kN	

TABLE VI
THE PEAK LOAD FOR IRREGULAR FEM MESH AND SPH PARTICLE DISTRIBUTION
DISTANCE BETWEEN SPH PARTICLES IN CLUSTER 10 MM

Parameter κ	FEM	SPH	experiment
0.6		130.66 kN	
0.8		125.88 kN	
1.0	129.32 kN	112.87 kN	127.73 kN
1.2		96.45 kN	
1.4		71.02 kN	

Table IV and Table V contain numerical values for peak load. The optimum values are once again close to 0.7. However, because peak load falls with growing intracluster distance between SPH particles, the κ value can also continue to fall.

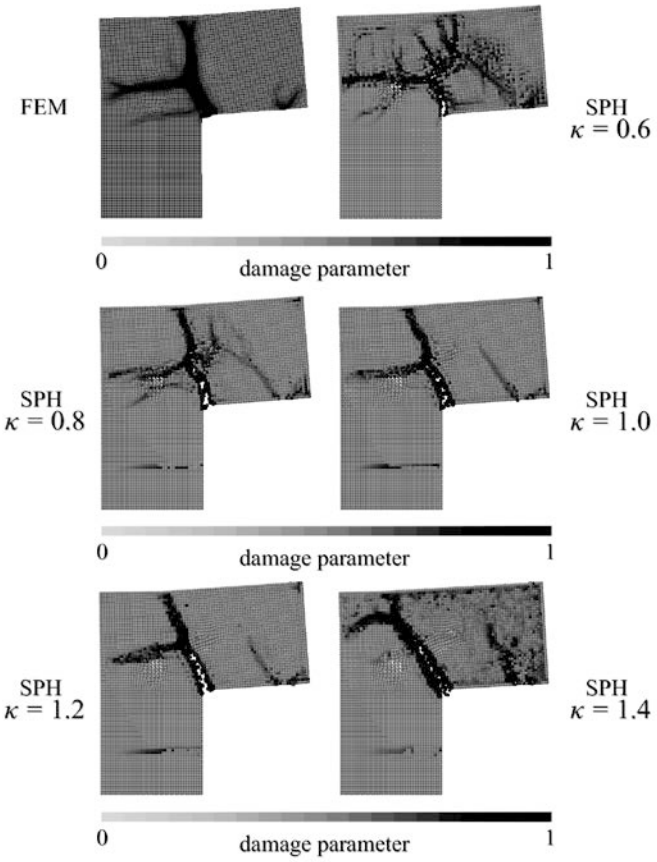

Fig. 9. Irregular FEM mesh and SPH particle distribution results. Distance between SPH particles in cluster 10 mm.

B. Function κ

In order to determine the beginning of the trend of function κ, the intracluster distance between particles is gradually lowered to the value at which distribution is regular. With regard to the scope of this contribution, Fig. 9 shows failures only for intracluster distances between particles of 10 mm. It is clear from the measured values in Table VI that for all values of κ the peak load values tend to return to the original peak load value (both from above and below) determined for regular particle distribution; see Table II.

In Fig. 10, function κ is compiled from the discussed results. The horizontal axis shows the percentually increasing difference in distances between SPH particles within the cluster zone and those in the rest of the model. With regard to the fact that clusters (irregular regions) were always inserted into a discretized body where the distance between SPH particles was 6.25 mm, $\kappa = 1$ is equal to 0 on the horizontal axis. In other words, a 100 % value on the horizontal axis means that the intracluster SPH particle distance was 12.5 mm.

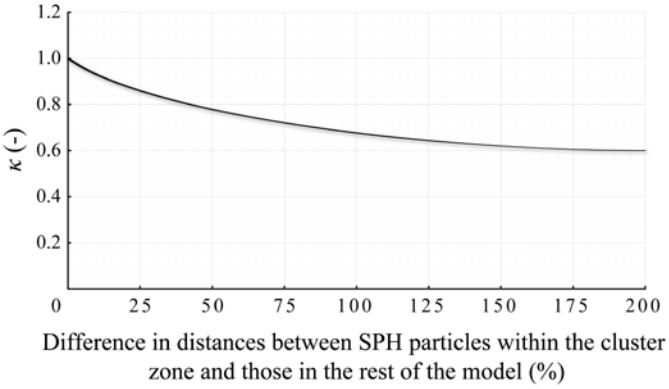

Fig. 10. Function κ.

VII. CONCLUSION

The regularity of the distribution of SPH particles plays a significant role in simulations which use the SPH method. In the cases of poor regularity and the use of quasi-brittle materials, unreal types of crack propagation can be expected. As a rule, cracks try to avoid areas where particle clusters occur. By choosing a suitable support domain size, results which correspond to those of experiments can be achieved. The size of the support domain can be reduced via parameter κ. It is apparent that the choice of $\kappa < 1$ helps to reduce the size of the impact of poor regularity in the distribution of SPH particles.

ACKNOWLEDGMENT

This outcome has been achieved with the financial support of project GACR 14-25320S “Aspects of the use of complex nonlinear material models” provided by the Czech Science Foundation; with the support of the project FAST-S-16-3718 “Advanced numerical methods with complex material models” provided by the Brno University of Technology fund for specific university research; and also with the support of the

project LO1408 "AdMaS UP – Advanced Materials, Structures and Technologies" provided by the Ministry of Education, Youth and Sports under the „National Sustainability Programme I".

REFERENCES

[1] Z. Kala, "Sensitivity and Reliability Analyses of Lateral-torsional Buckling Resistance of Steel Beams," *Archives of Civil and Mechanical Engineering*, vol. 15, no. 4, 2015, pp. 1098–1107.

[2] Z. Kala, "Reliability Analysis of the Lateral Torsional Buckling Resistance and the Ultimate Limit State of Steel Beams," *Journal of Civil Engineering and Management*, vol. 21, no. 7, 2015, pp. 902–911.

[3] J. Flodr, M. Krejsa, D. Mikolasek, J. Brozovsky, and P. Parenica, "Numerical modeling of a thin-walled profile with respect to the redistribution of bending moments," in *Proceedings of the Civil-Comp*, vol. 108, 2015.

[4] Z. Kala, "Global Sensitivity Analysis in Stability Problems of Steel Frame Structures," *Journal of Civil Engineering and Management*, vol. 22, no. 3, 2016, pp. 417–424.

[5] J. Protivinsky, and M. Krejsa, "Reliability Assessment of the Dissipative Link in Steel Boiler Structure with Regard to Seismic Load," in *Proceedings of the 4th International Conference on Materials Engineering for Advanced Technologies*, ICMEAT 2015, 2015, pp. 202–206.

[6] J. Kralik, "Safety of Nuclear Power Plants under the Aircraft Attack," *Applied Mechanics and Materials*, vol. 617, 2014, pp. 76–80.

[7] J. Kralik, and M. Baran, "Numerical Analysis of the Exterior Explosion Effects on the Buildings with Barriers," *Applied Mechanics and Materials*, vol. 390, 2013, pp. 230–234.

[8] J. Kralik, "Optimal Design of NPP Containment Protection Against Fuel Container Drop," *Advanced Materials Research*, vol. 688, 2013, pp. 213–221.

[9] P. Kral, J. Kala, and P. Hradil, "Verification of the Elasto-Plastic Behavior of Nonlinear Concrete Material Models," *International Journal of Mechanics*, vol. 10, 2016, pp. 175–181.

[10] J. Kala, and M. Husek, "Useful Material Models of Concrete when High Speed Penetrating Fragments are Involved," in *Proceedings of the 9th International Conference on Continuum Mechanics*, vol. 15, 2015, pp. 182–185.

[11] F. Hokes, J. Kala, and O. Krnavek, "Nonlinear Numerical Simulation of a Fracture Test with Use of Optimization for Identification of Material Parameters," *International Journal of Mechanics*, vol. 10, 2016, pp. 159–166.

[12] J. Kala, P. Hradil, and M. Bajer, "Reinforced concrete wall under shear load – Experimental and nonlinear simulation," *International Journal of Mechanics*, vol. 9, 2015, pp. 206–212.

[13] J. Kala, and M. Husek, "High Speed Loading of Concrete Constructions with Transformation of Eroded Mass into the SPH," *International Journal of Mechanics*, vol. 10, 2016, pp. 145–150.

[14] J. Kala, and M. Husek, "Improved Element Erosion Function for Concrete-Like Materials with the SPH Method," *Shock and Vibration*, vol. 2016, 2016, pp. 1–13.

[15] G. R. Liu, and M. B. Liu, *Smoothed particle hydrodynamics: a meshfree particle method*, New Jersey: World Scientific, 2003, 449 p., ISBN 981-238-456-1.

[16] W. Benz, "Smoothed particle hydrodynamics: a review," *NATO Workshop*, Les, Arcs, France; 1989.

[17] J. Ožbolt, N. Bede, A. Sharma, and U. Mayer, "Dynamic fracture of concrete L-specimen: Experimental and numerical study," *Engineering Fracture Mechanics*, vol. 148, 2015, pp. 27–41.

[18] Livermore Software Technology Corporation (LSTC), "LS-DYNA Theory Manual," LSTC, Livermore, California, USA, 2016.

[19] Y. D. Murray, "User's manual for LS-DYNA concrete material model 159," FHWA-HRT-05-062, 2007.

[20] Y. D. Murray, A. Abu-Odeh, and R. Bligh, "Evaluation of concrete material model 159," FHWA-HRT-05-063, 2006.